Bacterial cellulose/silica hybrid fabricated by mimicking biocomposites

**Hideaki Maeda · Megumi Nakajima ·
Toshiki Hagiwara · Takashi Sawaguchi ·
Shoichiro Yano**

Abstract In plants such as grasses, rice, and sugar cane, biomineralizatin occurs such that amorphous silica is drawn from soil, transferred and deposited on polysaccharide matrix. In this study, by mimicking natural biomineralization in plants, a cellulose/silica hybrid was produced using bacterial cellulose (BC). BC hydro-gel was immersed in an aqueous solution of silanol derived from tetraethoxysilane (TEOS), and silanol was then converted into silica in the BC hydro-gel matrix. By pressing the BC hydro-gels and hybrids at 120 °C and 1–2 MPa, water-free translucent sheets were obtained. In the leaves of rice plants, large silica bodies (μm order) were embedded in the polysaccharide matrix, whereas in the BC/silica hybrids, nano scale silica was embedded between the micro fibrils of the BC matrix. Reflecting this structure, the modulus of elasticity and tensile strength of dry BC/silica hybrid improved to 17 GPa at 25 °C and 185 MPa, respectively. In the case of rice plants, the modulus was 3.5 GPa at 25 °C and the tensile strength was 25–88 MPa, suggesting a weaker structure than in BC hybrid.

Introduction

Composite materials are fabricated by combining more than two materials, i.e. polymer/polymer, polymer/fiber, and polymer/mineral filler, and have excellent mechanical, thermal and chemical properties. Such composite materials have been successfully used as structural or packaging materials.

Composite materials having excellent performance, however, are frequently found in natural biological materials, which are produced by natural biomineralization. Bones, teeth, shells, eggs, grasses, and diatoms are typical examples of biocomposites. In biocomposites, minerals are deposited and grow in situ in natural polymer matrices under mild conditions, which control the biomineralization steps of nucleation, polymorph selection, crystal growth direction and crystallographic orientation of minerals [1].

These sophisticated biomineralization processes are difficult to realize in artificial systems. However, the recent interest in nanotechnology has stimulated much research in this area and various efforts have been made to prepare functional materials mimicking the structure, composition, process, and in situ deposition of biocomposites. Mann and his co-workers [2] investigated the concept of biomineralization of the nacreous inner surface of shell through the use of stearic acid monolayers during the controlled crystallization of $CaCO_3$ from supersaturated solutions. The presence of an organized monolayer gives rise to oriented vaterite formation, whereas in the absence of a monolayer, rhombohedral calcite crystals were formed.

The teeth of marine crustacea contain iron oxide and magnetotactic bacteria living in lake beds contain chains of magnetic iron oxide particles. In these cases, the oxide is formed from soluble precursors within a soft-tissue matrix. Using a similar method, Sobon et al. [3] produced polymethylmethacrylate (PMMA)/ferric oxide and PMMA/magnetite composites. They

H. Maeda · M. Nakajima · T. Hagiwara · T. Sawaguchi ·
S. Yano (✉)
College of Sci. and Technol., Nihon Univ., 1-8-14
Kanda-surugadai, Chiyoda-ku, Tokyo 101-8308, Japan
e-mail: yano@chem.cst.nihon-u.ac.jp

dissolved iron (III) chloride or iron (III) acetylaceto-nate with polymer in a solvent and cast sheets. These sheets were then treated with base to produce hydrated iron oxide, which was then converted into ferric oxide by heat treatment, or to magnetite by reduction or treatment with a ferrous salt solution.

Mimicking the biosynthetic mechanisms, Bianconi et al. [4] obtained poly(ethyleneoxide)(PEO)/CdS in situ composite. Crystal size, morphology, and orientation of CdS were controlled by a polymer matrix. Moyle [5] produced a composite containing non-linear optical crystals. Calvert and Broad [6] also produced composites with potassium dihydrogen phosphate in PEO by casting a sheet from aqueous solution. Particle size, shape, orientation and high particle loading were studied. Nucleation and growth of calcium carbonate crystals on surface-modified polyethylene and polystyrene were studied from the view point of biomineralization [7].

In the nacreos layer of abalone shell, the microstructure is highly ordered as $CaCO_3$ (aragonite) crystals, with a thickness of 250 nm, separated by a layer of organic matter 30–50 nm thick. Mimicking this biomineralization, Yasreb et al. [8] processed laminated B_4C/Al cermets. This cermets displayed a 40% increase in both fracture toughness and strength over monolithic B_4C/Al cermets. A dense, uniform and highly biologically active bone-like apatite layer could be formed in arbitrary thickness on any type and shape of solid substrate surface using biomimetic methods at ordinary temperature and pressure [9]. Biomineralization and biomimetic synthesis are reviewed elsewhere [1, 10–13].

In the present study, by mimicking the biomineralization in rice plants, cellulose/silica hybrid is produced. Generally, cellulose does not readily form composite materials, as it is insoluble in most solvents and also does not melt at elevated temperatures. In this study, bacterial cellulose (BC) hydro-gel is used as a matrix and BC gel/silica hybrids are fabricated. This process is distinguished from designing of other cellulosic composites. For example, solvent soluble cellulose derivatives such as hydroxypropyl cellulose (HPC) can be hybridized by the sol–gel process mixing HPC together with TEOS in solvent [14, 15]. Evaluation of the mechanical properties of BC hydro-gel and BC/silica hybrid was performed by compression creep in water. Furthermore, if BC hydro-gels and hybrids are pressed, dry BC and BC/silica hybrid sheets can be processed. The mechanical properties of these sheets were also evaluated and compared with those of rice plants.

Experimental

Preparation of BC

Culture medium was prepared by dissolving 15 g of glucose, 2.5 g of polypeptone, 0.5 g of $MgSO_4 \cdot 7H_2O$, 2.5 g of yeast-extract, and a small amount of vitamins (NEO M.V.I-9, SSP Co. Ltd.) in 500 cm^3 of water. After sterilizing this solution by heating at 120 °C for 9 min in an autoclave, 0.5% ethanol and 0.5 g of mannitol were added. Culture was carried out under static conditions in a glass vessel (100 mm diameter × 600 mm depth) at 30 °C for 25 days by adding activated seed broth. First, the solution became turbid, a pellicle appeared on the surface of the liquid and pellicle thickness increased gradually, reaching 20–30 mm after 25 days. The species of bacteria was *Gluconacetobacter xylinus* (IFO 13772). For purification, after washing the obtained BC hydro-gel in water, it was immersed in 1% aqueous NaOH for 1 day, followed by 1% aqueous $NaClO \cdot 5H_2O$ for 1 day.

Preparation of BC/SiO$_2$ hybrid

Tetraethoxysilane (TEOS) was mixed with 100 g of water together with 0.1 N acetic acid and was allowed to stand for about 1 h with stirring. TEOS was converted into aqueous silanol sol. In order to control the silica content in BC gel, TEOS concentration in water was varied, i.e. 10 or 20%. BC gels of 30 × 30 mm (thickness, about 20–30 mm) were immersed in 100 cm^3 aqueous silanol solution and allowed to stand for 2–3 days. Absorbed silanol (≡ SiOH) in BC gels were converted to silica by polycondensation reaction, and BC gel/silica hybrid was prepared, as shown in Fig. 1. This process mimicked biomineralization in rice plants, absorbed silica was deposited in situ into a BC gel matrix.

In order to obtain dry BC/silica hybrids, BC hydro-gel were immersed in various concentrations of aqueous silanol solutions changing TEOS content as 0.05–0.3 wt%. At high concentration of TEOS more than 10 wt%, very brittle dry BC/silica hybrids are obtained. Dry BC or BC/silica hybrid sheets were obtained by pressing BC or BC/silica hydro gels at 120 °C and 1–2 MPa. In this manner, dry BC/silica hybrid sheets containing 4.1, 5.3, and 7.1 wt% of silica were produced, and were named as BC/S-1, BC/S-2, and BC/S-3, respectively.

Fig. 1 Preparation of BC
hydro-gel/silica hybrid and
dry BC/silica hybrid sheet
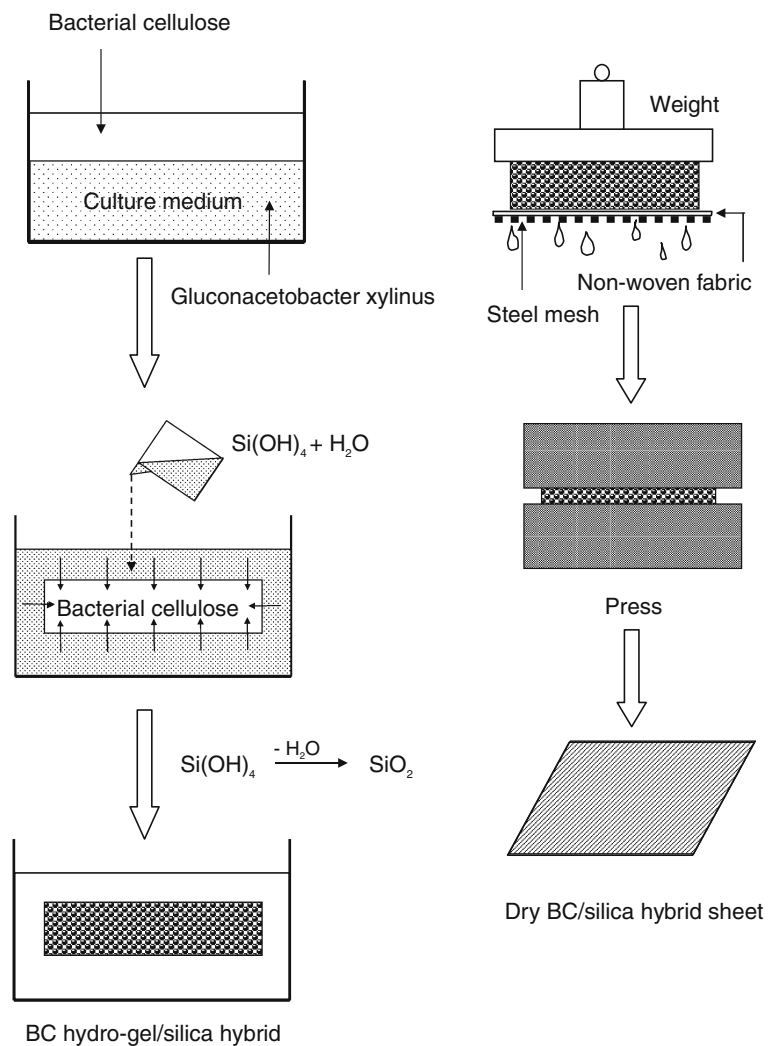
Measurements

Creep

The mechanical properties of BC gel and BC gel/silica hybrids were evaluated by compression creep in water. Figure 2 shows a creep apparatus. BC gels ($20 \times 20 \times 20$ mm) were placed in vessels together with water. A constant load of 50 g, including the weight of the device, was applied to the sample, as shown in Fig. 2. Deformation γ $[= (l_0 - l)/l_0]$ was determined as a function of time using a cathetometer, where l_0 is the initial thickness of sample and l is the thickness at time t. Water in the vessel was regulated by circulating water at constant temperature.

Dynamic viscoelasticity

The dynamic viscoelastic properties of rice plant, dried BC and BC/silica hybrid samples were measured using

a dynamic viscoelastic analyzer (IT Keisoku Co. DVA-200) at a frequency of 10 Hz. The storage modulus, E', and loss tangent, $\tan \delta$, were measured as a function of temperature at a heating rate of 2 °C/min.

Stress–strain measurement

The tensile properties of rice plant, dried BC and BC/silica hybrid samples were measured using a IM-20 (INTESCO Co., Ltd.). The cross-head speed was
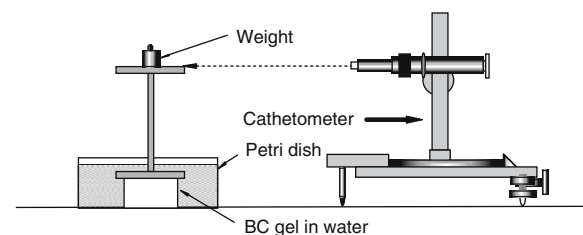

Fig. 2 Compression creep measurement of BC hydro-gel and its hybrid in water

10 mm/min and the gauge length was 20 mm. Rectangular specimens of 30 × 50 mm were used.

X-ray diffractometry

X-ray diffractometry was performed using an X'Pert PRO MPD (Panalytical). The X-ray generator was operated at 40 kV and 40 mA, and a Ni filtered Cu Kα beam with a wave length of 0.154 nm was used.

Scanning electron microscopy (SEM)

SEM observation was carried out by using an Akashi ALPHA-30A at 25 kV. Samples were mounted on an aluminum stub and coated with a thin layer of gold by using an ion-coater model 1B-3 (Eiko-Engineering Co., Ltd.).

Results and discussion

Biomineralization of rice plant

In grasses such as rice plant, silica is supplied by soil in the form of hydrated silica, transferred and accumulated as amorphous silica (opal) on the polysaccharide matrix in shoots. In the case of diatoms, cell walls and cell contents are constituted of polysaccharide and protein. Hecky et al. [16] hypothesized that the protein served as a template for silica mineralization. Serine and threonine, having hydroxyl-containing side chains, undergo condensation reactions with silicic acid ($Si(OH)_4$ or $SiO_2 \cdot 2H_2O$), and are fixed to the protein template, as shown in Fig. 3. It is believed that the structure of silica is controlled by the arrangement of amino acids.

In the shoot epidermal system, silica becomes localized in stomata, silica cells, trichomes and long cells [17]. Accumulated silica in the shoots functions to provide support to the shoot system, to deter predators and to conserve water during moisture stress [17]. It is also reported that silica cells, filled with silica gel, provide windows in the epidermal system, allowing more light to be transmitted to photosynthetic mesophyll and cortical tissue below the epidermis in the leaves and stems, respectively [18]. Silica in rice plants is considered to be an essential element, although the beneficial effects of silica on growth and yield are partly attributed to the effects of the element on protecting plant from fungal diseases and insects [18, 19].

Figure 4 shows SEM micrographs of rice plant leaves, which were harvested in autumn 2003 in Tsukuba-shi, Ibaraki, Japan. (a) and (b) are SEM images of the leaves before sintering. Silica embedded in polysaccharide matrix are observed. Branches of silica protrude beyond the surface. Micrographs (c) and (d) are sintered samples of (a) and (b), respectively. Branched silica rods of about 4 μm in diameter, with small branches of about 2 μm, can be seen. This type of branched silica was also observed in the adaxial epidermis of *Nardus stricta* (*Gramineae*) [20].

Rice plants contain 40.3% cellulose, 26.2% pentosans, 21.2% lignin and 13–16% ash (silica) [21]. Cellulose in rice plants may be amorphous, as can be seen in the X-ray diffraction pattern (Fig. 5). The X-ray diffractogram of rice plant did not show the pattern of cellulose I, which is usually observed in natural polysaccharides, such as bacterial, *Valonia*, cotton, wooden and ramie celluloses.

The mechanical properties of the rice plant were evaluated. Figure 6 shows the dynamic viscoelastic properties of the lower and upper parts of stalks, and the ears of the rice plant. The storage modulus E' of rice plant in the glassy state were rather low when compared with those of cellulose I (BC), because cellulose in rice plants is amorphous, as shown in Fig. 5. E' was 5 GP at −145 °C and 2 GPa at 280 °C, and the temperature dependence of E' was very small over the wide temperature range from −145 to 280 °C. E' decreased sharply above 280 °C due to glass transition and/or thermal degradation. E' of the lower part of stalk was higher than that of the upper part of stalk and ears. This may be due to the silica content of the rice plant. The lower part of stalk contains 14.7 wt% silica, which is higher than the upper part (13.0 wt%) and ears (13.5 wt%). The lower part of stalk, which is close to the roots, may be reinforced by higher silica content. In the tan δ curves, peaks appeared at about −100, 100,

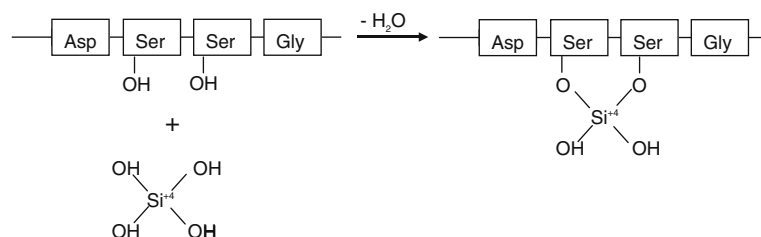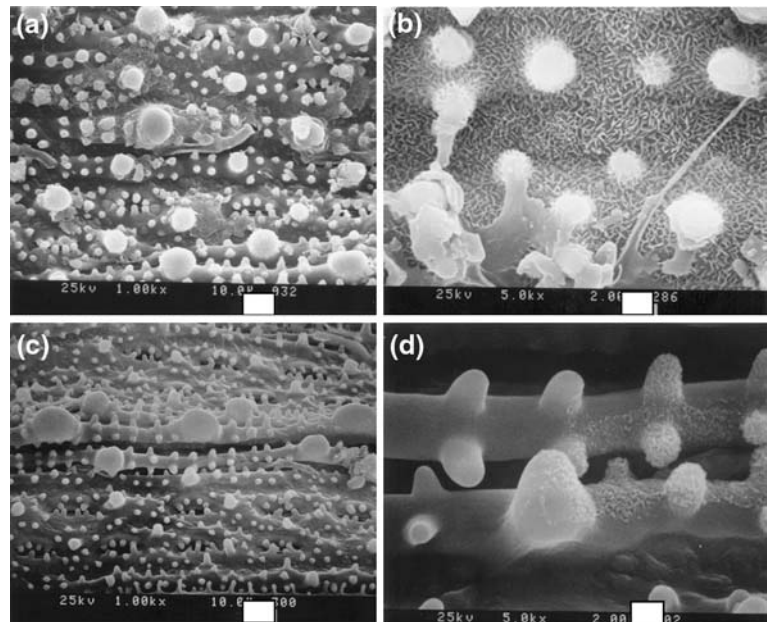**Fig. 3** Reaction between silica acid and protein template [16]

Fig. 4 SEM images of rice plant leaves. (**a**) Before sintering, magnification 1,000×, scale bar 10.0 μm; (**b**) before sintering, magnification 5,000×, scale bar 2.0 μm; (**c**) after sintering, magnification 1,000×, scale bar 10.0 μm; and (**d**) after sintering, magnification 5,000×, scale bar 2.0 μm

and 250 °C. The peak at −100 °C is caused by local mode motion of glucose units [22] that at about 100 °C may be due to evaporation of adsorbed water. Because the glass transition temperature of cellulose is reported to be about 250 °C, but degradation also occurs at 250 °C [22], the peak at 250 °C is associated with both glass transition and thermal degradation.
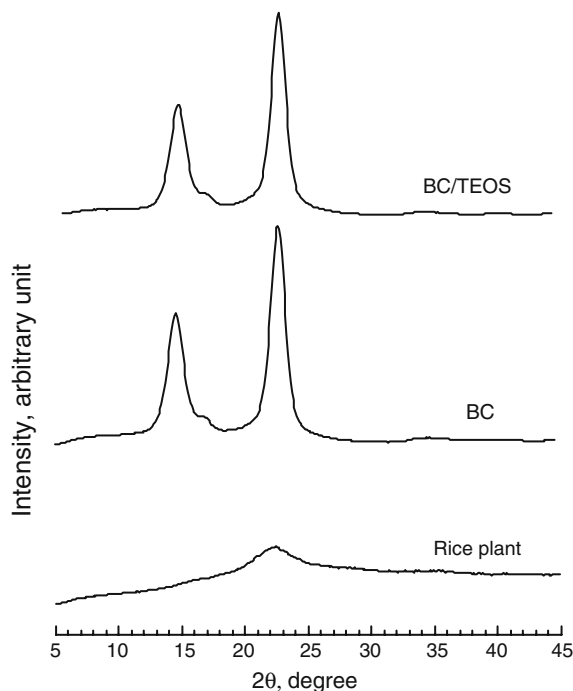
Figure 7 shows the stress–strain curves of the lower and upper parts of stalks and ears of the rice plant. The ultimate strength of the lower part of stalk was higher when compared with the upper part of stalk and ears, largely due to silica content. However, the strength of ears was very poor, despite containing 13 wt% silica. This may be caused by the complex shape of the ear, where stress concentration occurs. The mechanical properties of the rice plant at room temperature are almost the same as polystyrene, polymethyl methacrylate and poly(vinyl chloride).
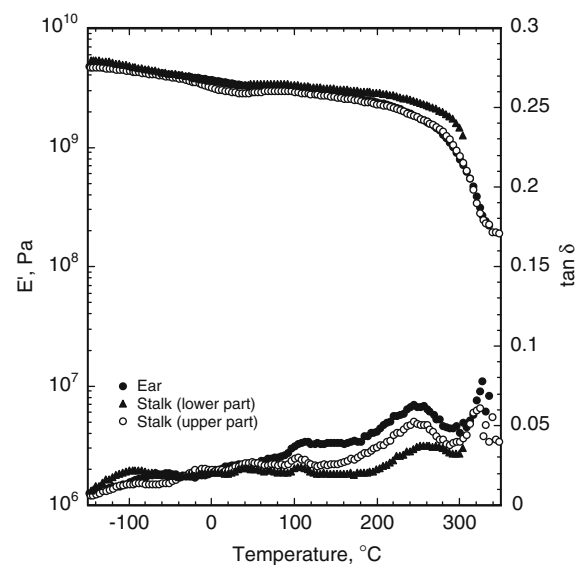

Fig. 5 X-ray diffraction patterns of BC/TEOS hybrid, BC and rice plant (leaves)

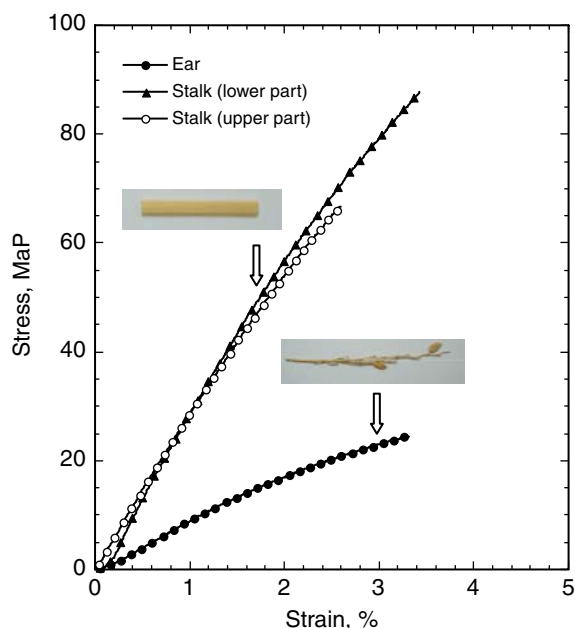**Fig. 6** Dynamic viscoelasticity of rice plant

Fig. 7 Stress–strain curves of various parts of rice plant

Structure of BC and BC/Silica hybrid

When culture is carried out using *Gluconacetobacter xylinus*, cellulose hydro-gel is obtained. Figure 8 shows scanning electron micrographs of pressed and dried BC sheet. Three-dimensional networks of fine micro-fibrils of about 10 nm develop, forming a porous structure of about 100 nm–1 μm. When processed into dried sheets, this structure reflects the structure of BC hydro-gel. Because spaces between micro-fibrils in BC hydro-gel are filled with water and because BC swells, the net content of cellulose in the hydro-gel is less than 1 wt%.

The X-ray diffractograms of pressed and dried BC sheets are given in Fig. 5. Dried BC sheet shows a typical cellulose I pattern with peaks appearing at $2\theta = 12$, 15 and 22° reflected from the (1$\bar{1}$0), (110) and (200) planes, respectively. In the case of BC, diffraction intensity at $2\theta = 12$° is strong and the (1$\bar{1}$0) plane of BC crystallite shows selective and strong plane orientation to the surface of micro-fibrils [23].

In order to produce the BC hydro-gel/silica hybrid, BC hydro-gel was immersed in a silanol sol prepared from TEOS dispersed in water using acetic acid as a catalyst. The process of preparation of the BC hydro-gel/silica hybrid, and dried and pressed sheets, is shown in Fig. 9. Silanol sol is diffused and penetrates into the spaces between cellulose micro-fibrils. It is known that silanol is reactive and reacts with hydroxyl groups on organic polymers such as poly(vinyl alcohol) [24], or polydimethylsiloxane having hydroxyl groups on both chain ends [25] in organic–inorganic hybrids, and also
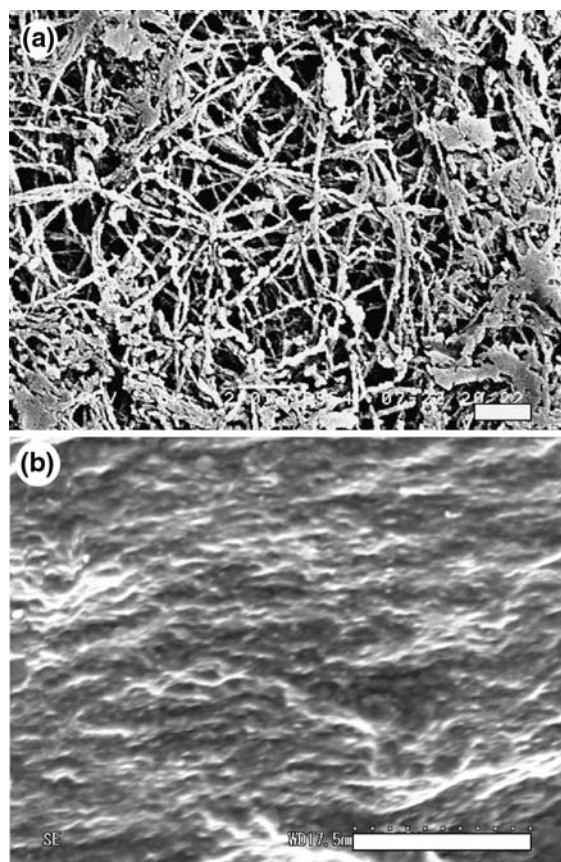

Fig. 8 SEM images of BC and hybrids. (a) Dry BC sheets (magnification 2,000×); (b) after sintering BC/silica hybrid at 500 °C in air (cross-sectional surface, magnification 2,000×)

in biocomposite such as diatoms [16]. Therefore, cellulose micro-fibrils having hydroxyl groups may undergo condensation reactions with supplied silanol, which becomes fixed to micro-fibrils, as in the case of diatoms (Fig. 3). Silanol itself also condenses forming silica, and is deposited on cellulose micro-fibrils through hydrogen bonding or condensation reactions with cellulose. Figure 8 shows SEM images of the cross-sectional surface of pressed and dried BC/silica hybrid sheets after sintering at 500 °C in air. Silica converted from TEOS may be embedded in the spaces between micro-fibrils during hybridization, and wrinkling patterns of about 5–10 μm can be seen. This pattern reflects the spaces between micro-fibrils. Silicification occurs in situ on cellulose micro-fibrils similarly as biomineralization in rice plants.

In the present study, BC hydro-gel was immersed into 10 and 20% aqueous TEOS dispersions and silica was finally deposited on BC micro-fibrils via silanol. In order to determine the amount of silica in BC sheets, TG measurement was carried out in air. Figure 10 shows the TG curves of BC and BC/silica hybrids prepared by immersing the BC hydro-gels into 10 and 20%

Fig. 9 Preparation process of dry and pressed BC/silica hybrids from BC hydro-gels
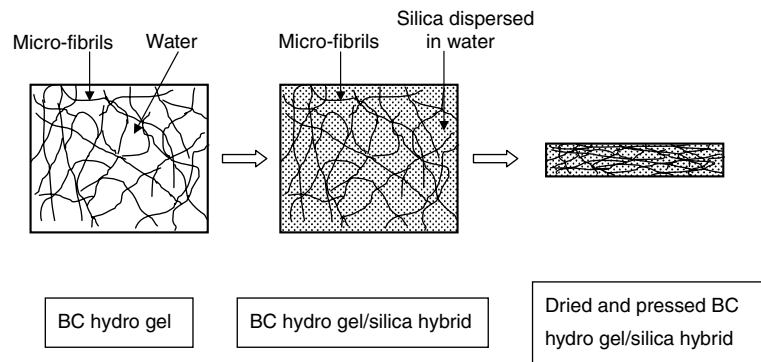
of TEOS. In both samples the thermal degradation of BC occurs at about 320 °C. Residual weight above 500 °C was determined as silica content of the hybrids. Hybrids prepared from 10 and 20% TEOS contained about 39 and 43 wt% silica, respectively.

The X-ray diffractogram of BC processed into sheets is shown in Fig. 5. BC/silica hybrid from 20% TEOS shows a cellulose I pattern and strong planer orientation of the $(1\bar{1}0)$ plane is observed. The crystal structure of BC micro-fibrils is not affected by hybridization.

Compression creep

The mechanical properties of BC hydro-gels and silica hybrids were evaluated by simple compression creep measurement in water. Figure 11 shows the compression creep of BC hydro-gel in water as a function of temperature. A weight of 50 g, including the device, was

loaded onto the BC hydro-gel sample and deformation was read as a function of time using a cathetometer, as shown in Fig. 2. The strain $\gamma(t) = (l_0 - l)/l_0$ was plotted against time t. It is known that the creep behavior of polymers can be expressed by a Voigt model. In the present case of BC hydro-gel, the creep behavior during the experiment can be approximated by two Voigt models combined in series, as is given in Fig. 12. The compression strain $\gamma(t)$ can be given by the following equation

$$\gamma(t) = \gamma_1[1 - \exp(-t/\lambda_1)] + \gamma_2[1 - \exp(-t/\lambda_2)]. \quad (1)$$

Equation 1 can be rewritten as Eq. 2

$$\gamma(t) = \gamma(\infty) - \gamma_1 \exp(-t/\lambda_1) - \gamma_2 \exp(-t/\lambda_2), \quad (2)$$

where, $\gamma(\infty) = \gamma_1 + \gamma_2$ is the equilibrium value at $t = \infty$ and λ_1 and λ_2 are the retardation times. Retardation times λ_1 and λ_2 are calculated as follows, if λ_1 is the
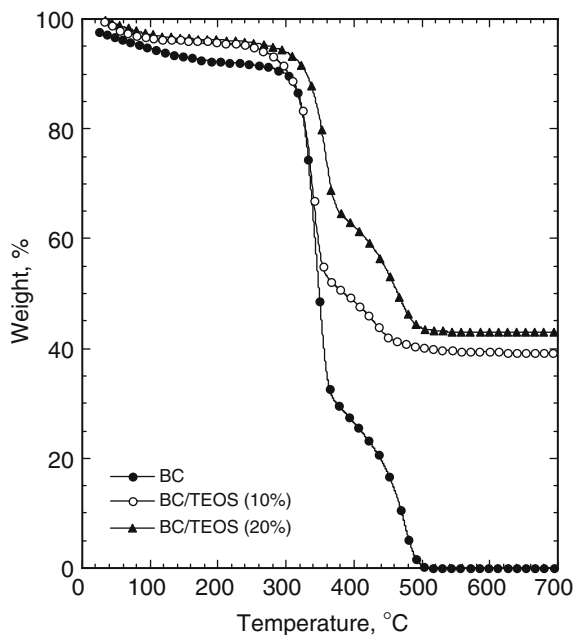

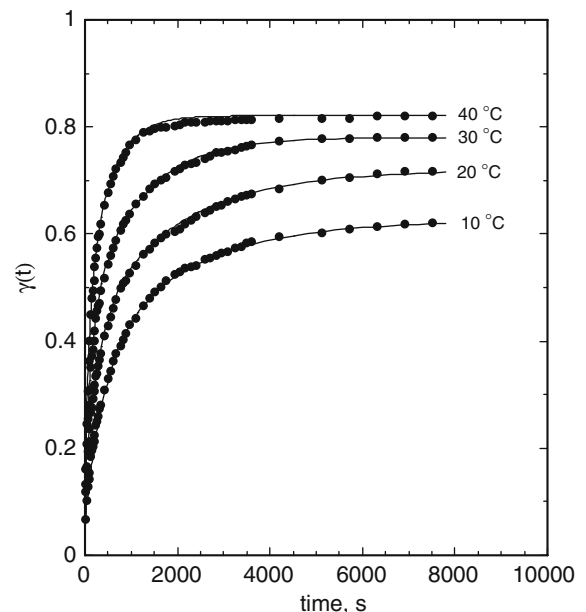**Fig. 10** TG curves of BC and dry BC/silica hybrids in air

Fig. 11 Compression creep of BC hydro-gel in water as a function of temperature
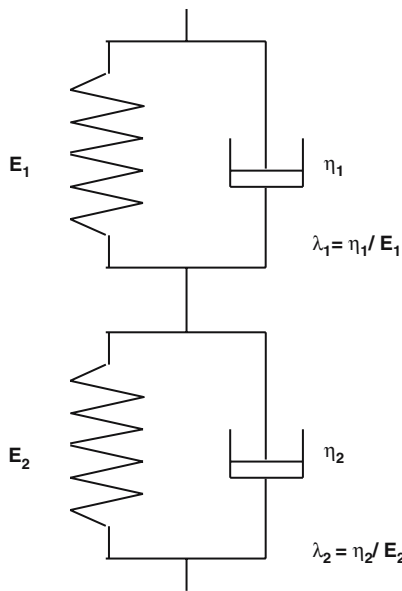
Fig. 12 Voigt model for creep behavior of BC hydro-gel

Fig. 13 Analysis of creep behavior of BC at 20 °C based on Eq. 1

short retardation time and λ_2 is the long retardation time, λ_1 is negligible at longer times, and Eq. 2 can be approximated by Eq. 3.

$$\gamma(\infty) - \gamma(t) = \gamma_2 \exp(-t/\lambda_2). \tag{3}$$

As shown in Fig. 13, when $\ln[\gamma(\infty) - \gamma(t)]$ is plotted against t, a straight line is obtained in the longer time region. From the slope and intercept of the straight line, $1/\lambda_2$ and γ_2 are obtained, respectively. Then, $1/\lambda_2$ and γ_2 are substituted in Eq. 2, and if $\ln[\gamma(\infty) - \gamma(t) - \gamma_2 \exp(-t/\lambda_2)]$ is plotted against t, another straight line is obtained at the short time region (Fig. 13). From the slope and intercept of the straight line, $1/\lambda_1$ and γ_1 are obtained, respectively. Temperature dependence of the retardation times is shown in Table 1. Solid lines in Fig. 11 are calculated values of $\gamma(t)$ substituting γ_1, γ_2, λ_1 and λ_2 in Eq. 1. Calculated values correlate well with experimental values.

The Arrhenius equation for temperature dependence of λ is given by Eq. 4.

$$1/\lambda = A \exp(-E_a/RT), \tag{4}$$

where A is constant, E_a is the activation energy and R is the gas constant. Figure 14 shows the Arrhenius plots of the retardation times of BC, calculated based on Eq. (4), against the reciprocal of absolute temperature. The retardation times and the apparent activation energies are summarized in Table 1.

The apparent activation energies are obtained as 19.3 kJ/mol for λ_1 and 18.0 kJ/mol for λ_2, as shown in Table 1. These values agree with the activation energy
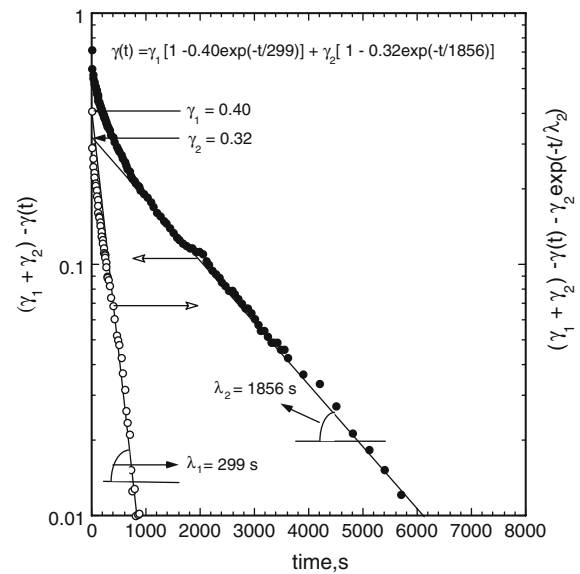
Table 1 Temperature dependence of λ_1 and λ_2

	40 °C	30 °C	20 °C	10 °C	E_a (kJ/mol)
λ_1 (s)	86	163	299	399	19.3
λ_2 (s)	478	1,113	1,856	1,934	18.0

for hydrogen bond formation [26]. The rate of deformation of BC hydro-gel is determined by hydrogen bonding between cellulose micro-fibrils. When force is applied to BC gel, micro-fibrils are directed toward the stable position, forming hydrogen bonds. The rate of deformation of fibrils changes with elapsed time. Creep deformation occurs as a two-stage process during
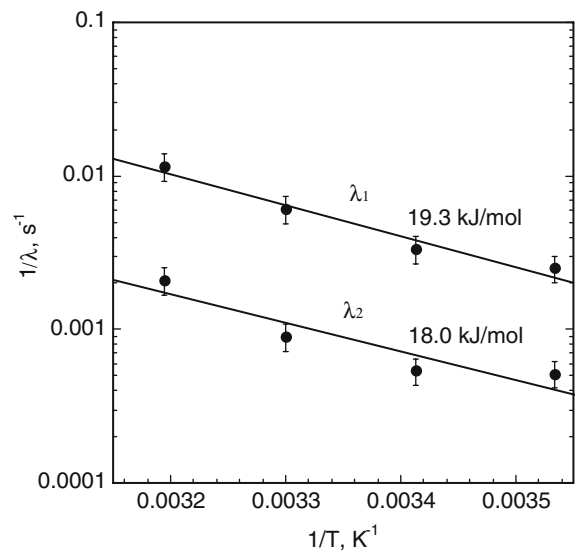

Fig. 14 Arrhenius plots for creep data of BC in water

observation. At the initial stage of loading, deformation occurs rapidly (corresponding to λ_1). Hydrogen bonds are gradually formed during loading, and the deformation rate slows (corresponding to λ_2), as the formed hydrogen bonds restrict the motion of fibrils.

Figure 15 shows the creep curves of BC gels and BC gel/ silica hybrids in water at 20 °C as a function of initial TEOS content. Deformation of BC gel/silica hybrids decreases with increasing initial TEOS content. Deposited silica in situ in BC gels reinforced the BC gel hybrids and suppressed deformation of the BC gels. As listed in Table 2, the retardation times of the BC gel/silica hybrids are longer than those of BC gels, as deformation of the micro-fibrils may be restricted by silica deposited between fibrils and more time is needed to reach equilibrium.

Dynamic viscoelastic properties of dry BC and BC/ silica hybrids

BC hydro-gel contains 99.8% of water, and by pressing BC gels at 120 °C for 10 min, water-free translucent BC sheet was obtained. BC/silica hybrid sheets could also be obtained by pressing BC gel/silica hybrids. When the BC hydro-gels were immersed in 10 and 20% aqueous TEOS solutions, 39 and 43% silica was deposited in dry BC hybrids, respectively as is seen in Fig. 10. A suitable amount of silica in hybrids for reinforcement is about 5–20 wt% [27, 28]. Large amounts of silica lead the hybrid becoming very brittle. In this study, to prepare BC hybrids with low concen-
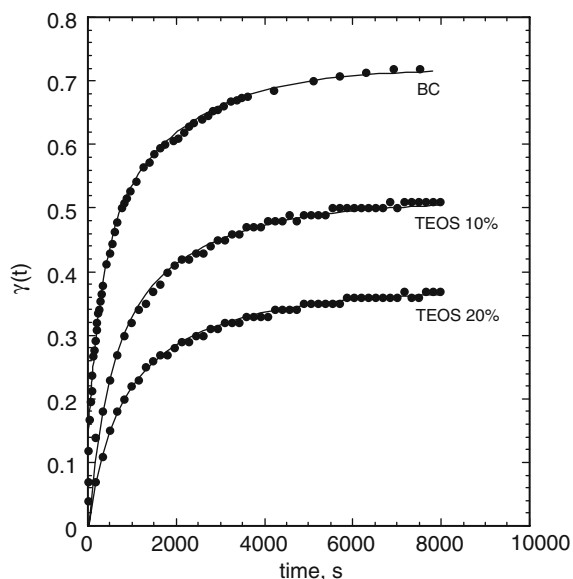
Table 2 Retardation times of BC gel/silica hybrids

	λ_1 (s)	λ_2 (s)
BC gel	299	1,856
BC gel/TEOS 10%	460	2,136
BC gel/TEOS 20%	483	2,234

trations of silica, BC hydro-gel was immersed in 0.05–0.3 wt% aqueous solutions of TEOS, and the hybrids containing 4.3–7.1 wt% of silica were obtained as can be seen in Table 3. However, it is very difficult to control precisely the loading amount of silica in the BC hydro-gel hybrids, because the concentration of the cellulose component in the hydro-gel varies depending on preparation conditions. BC/silica hybrid samples containing 4.3–7.1 wt% of silica were used for mechanical evaluation.

Figure 16 shows the dynamic viscoelastic properties of dry BC/silica hybrid sheets as a function of silica content. From −125 to 240 °C, E' decreased gradually and remained 10 GPa order, even at 240 °C showing good dimensional stability. In tan δ curves, small peaks appears at −80 and 100 °C due to local mode motion of glucose units and evaporation of water, respectively. At about 250 °C, no peak due to glass transition, which appeared clearly in rice plants (Fig. 6), was observed in BC samples. The intensities of these peaks decreased with silica content. The modulus of the hybrids almost systematically increased with SiO_2 content. The order of modulus at 200 °C was BC < BC/S-1 (SiO_2 content = 4.1%) < BC/S-2 (SiO_2 content = 5.3%) < BC/S-3 (SiO_2 content = 7.1%). While in the glassy state at 25 °C, the hybrids had the same E' value (17 GPa). The modulus of the BC/silica hybrid sheets was much higher when compared with rice plants, as shown in Table 3.

Figure 17 shows the stress–strain curves of dry BC/silica hybrid sheets as a function of silica content. The tensile strength of dry BC sheet was about 147 MPa, but that of the hybrids were increased by loading silica, i.e. 161 MPa at 5.3% silica and 185 MPa at 7.1% silica. The tensile strength of dry BC/silica hybrid sheets was stronger than that of rice plant as shown in Table 3.

Conclusions

Mimicking biomineralization in rice plants, cellulose/ silica hybrids were produced by the sol–gel process. BC hydro-gel was immersed in an aqueous solution of silanol derived from aqueous TEOS, which is converted to silica in situ in BC hydro-gels. BC hydro-gel/ silica hybrids were thus produced. The mechanical properties of the BC hydro-gels and BC hydro-gel/sil-

Fig. 15 Compression creep of BC hydro-gel and BC hydro-gel/ silica hybrids in water at 20 °C

Table 3 Mechanical properties of rice plant and BC/silica hybrids

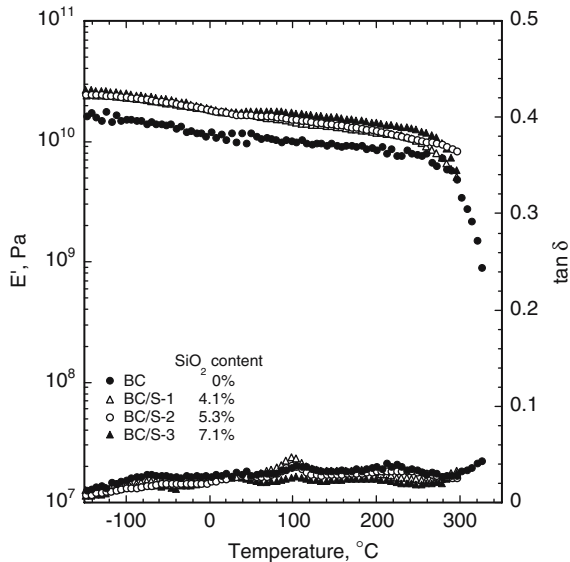|	SiO$_2$ content (%)	E' at 25 °C (Gpa)	E' at 200 °C (Gpa)	Strength (MPa)	Elongation (%)
BC sheet	0	11.8	8.4	147	2.5
BC/S-1	4.1	17.4	11.8	185	3.3
BC/S-2	5.3	17.1	12.2	161	2.0
BC/S-3	7.1	17.3	14.2	185	3.1
Rice plant					
Upper stalk	13.0	3.0	2.3	67	3.3
Lower stalk	14.7	3.5	2.9	88	2.6
Ear	13.5	3.5	2.4	25	4.1

Fig. 16 Dynamic viscoelasticity of dry BC/silica hybrids as a function of silica content
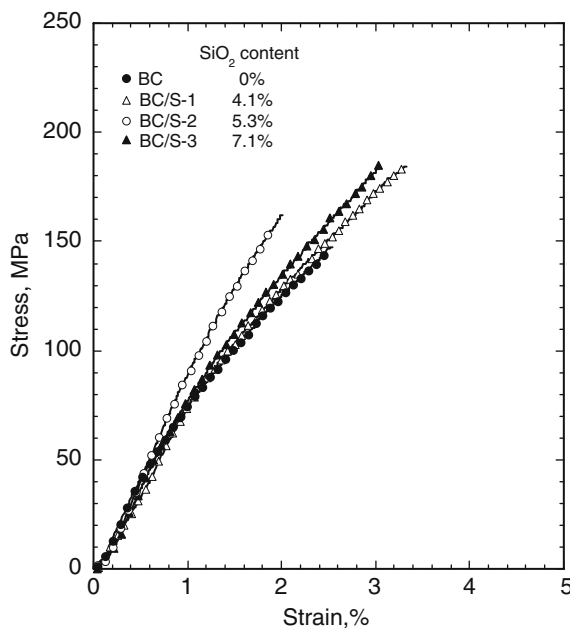

Fig. 17 Stress–strain curves of dry BC/silica hybrids as a function of silica content

ica hybrids were evaluated by the compression creep in water. The creep behavior of BC and its hybrids was approximated by two Voigt models having two retardation times, λ_1 and λ_2. Activation energies were calculated as 19.3 and 18.0 kJ/mol for λ_1 and λ_2, respectively.

Dry BC sheets were obtained by pressing BC hydrogels at 120 °C and 1–2 MPa for 10 min. The modulus of dry BC was 11.8 GPa at 25 °C and increased to 17 GPa by loading silica. The modulus of the hybrid was higher than that of dry rice plant stalk. The tensile strength of BC was 147 MPa and this increased to 160–185 MPa with increasing silica content. The tensile strength of rice plant was 25–88 MPa, which was lower than that of BC hybrids. It was found that deposited silica between BC micro-fibrils reinforced the hybrids.

References

1. Calvert P, Mann S (1988) J Mater Sci 23:3801
2. Mann S, Heywood BR, Rajam S, Birchall JD (1988) Nature 334(25):692
3. Sobon CA, Bowen HK, Broad A, Calvert PD (1987) J Mater Sci Lett 6:901
4. Bianconi PA, Lin J, Strzelecki AR (1991) Nature 349(24):315
5. Moyle BD, Ellul RE, Calvert PD (1987) J Mater Sci Lett 6:167
6. Calvert PD, Broad A (1988) In: Aksay IA, McVay GL, Stoebe TG, Wager JF (eds) Atomic & molecular processing of electromic and ceramic materials: preparation, characterization & properties, Material Research Society, Pittsburgh, Pennsylvania, p 89
7. Riehe PC (1988) ibid p.107
8. Yasrebi M, Kim GH, Gunnison KE, Milius DL, Sarigaya M, Aksay IA (1990) Mater Res Soc Proc 180:625
9. Takahasi M, Yao T, Kokubo T, Minoda M, Miyamoto T, Nakamura T, Yamamoto T (1995) J Biomedical Mater Res 29:349
10. Mann S (2004) Chem Commun (1):1
11. Nedoluzhko A, Douglas T (2001) Focus on biotechnology, vol 7. Physics and Chemistry, Basis of Biotechnology, p 9

12. Mann S (1995) J Mater Chem 5(7):935
13. Mann S (1993) Nature 365(6446):499
14. Yano S (1994) Polymer 35:5565
15. Yano S, Kodomari M (1996) Nihon Reoroji Gakkaishi 24:15
16. Hecky RE, Mopper K, Kilham P, Degens ET (1973) Mar Biol 19:323
17. Kaufman PB, Takeoka Y, Carlson TJ, Bigelow WC, Jones JD, Moore PH, Ghosheh NS (1979) Phytomorphology 29:185
18. Yoshida S, Onishhi Y, Kitagishi K (1959) Soil Plant Food 5:127
19. Yamamoto K, Baba A, Igarashi T (1957) Niigata Daigaku Nogakubu Gakujutsu Hokoku 9:26
20. Parry DW, Smithon F, (1964) Ann Bot N S 28:169
21. Jabbar MA, Serajul H (1973) Dacca Univ Stud 21(2, PtB):51
22. Nakamura S, Gillham JK, Tobolsky AV (1970) Rep Prog Polym Phys Jpn XIII:89
23. Takai M, Tsuta Y, Hayashi J, Watanabe S (1975) Polymer J 7:157
24. Hino T, Mochida K, Okamoto S (1983) Jap J Polym Sci Technol 40:225
25. Huang HH, Orler B, Wilkes GL (1985) Polym Bull 14:557
26. Moore WJ (1962) Physical chemistry, Maruzen Co. Ltd., p 550
27. Yano S, Iwata K, Kurita K (1998) Mater Sci Eng C6:75
28. Yano S, Kurita K, Iwata K, Furukawa T, Kodomari M (1998) Polymer 44:3515